USE OF EXTENDED POD TO ANALYSE A MULTI-SENSOR MEASUREMENTS IN A SEPARATED TURBULENT FLOW

C. HOARAU, L. DUONG , J. BORÉE, J. LAUMONIER, Y. GERVAIS
Laboratoire d'Études Aérodynamiques (LEA UMR 6609),
Téléport 2 , 1 Av. Clément Ader, BP 40109, 86961
Futuroscope Chasseneuil , FRANCE
cedric.hoarau@lea.univ-poitiers.fr

ABSTRACT

Wall pressure array measurements and LDV single point measurements of the velocity obtained on a 30° forward facing ramp are discussed in this paper. Mean and fluctuating signals are analyzed both in the mean separated region and in the recovering boundary layer flow. The results evidence the signature of both flapping and vortex shedding mechanisms in agreement with classical references. POD and Extended POD are then used to educe the length and time scale contribution of the shear layer structures on the pressure trace downstream of separation. We prove that the correlated pressure signal downstream the mean separation length carries the properties of the distorted mixing layer eddies being advected and dissipating in the outer boundary layer flow. A simple physical model is proposed.

INTRODUCTION

Understanding the intrinsic spatial and unsteady features of separated and reattaching flows has a great importance for the design and the control of a huge amount of engineering applications. These concern both external and internal aerodynamics because such regions have a major impact on aerodynamic performances, wind loading structures, efficiency of combustors, noise emissions, ...

The vast majority of the experimental and computational studies involves a bidimensionnal mean flow and separation from a sharp edge (Eaton and Johnston 1981; Kiya and Sasaki 1983; Cherry, Hillier and Latour 1984; Lee and Sung 2002) the separation bubble being an overwhelming perturbation to the boundary layer. In the separated region the signature of vortex shedding and flapping of the separation is detected. The phase relation, measured via wall pressure array messurements are different for these shedding and flapping mechanisms (Lee and Sung 2002; Hudy, Naguib and Humphreys 2003) and there are still unsolved questions regarding the feedback mechanism of the flapping motion. Downstream of the mean reattachment, the outer layer of the boundary layer is perturbed by large eddies generated in the separation region and transported downstream (Castro and Epik 1998; Song, DeGraff and Eaton 2000). Being able to educe the length and time scale contribution of these decaying structures on the pressure trace downstream of separation is an important issue for application.

The recent work of (Lee and Sung 2002) stresses the interest of multiple arrayed pressure measurements as a detection method for coherent structures. This appears as a first step for control purposes. A "spatial box filtering" is proposed in their paper as an inner product between the pressure distribution and an "ad hoc" square wave spatial filter function in the separated region downstream of the backward facing step. Our goal in this paper is to propose an alternative approach based on Extended Proper Orthogonal Decomposition (EPOD) - see (Borée 2003). Wall pressure array measurements combined with single point measurements of the velocity using two-composents Laser Doppler Anemometry have been obtained on a 30° ramp. The POD is first applied to the pressure signals under the separated bubble and we obtain an optimal basis for the decomposition of the unsteady pressure field at the source of the large scale perturbations. EPOD then enables us to deduce the only contribution to the fluctuating pressure or velocity field downstream correlated with the basis. The spectral characteristics of both correlated and uncorrelated signal will be studied in detail for the pressure measurements at increased distances from the separated bubble. A simple physical model is proposed. Our goal is mainly to show the potential of this eduction technique in a well defined and relatively simple 2D geometry.

1 DESCRIPTION OF THE EXPERIMENT

The experiments are performed in an anechoic open throat wind tunnel. The square nozzle section has dimensions of $400mm \times 400mm$. The test model is a forward facing ramp (See Fig. 1) of height $H = 50mm$ and width $l = 750mm$ with an angle of 30° at the foot's ramp. The distance between the foot ramp and the inlet duct is $300mm$ and the boundary layer displacement thickness at the exit nozzle is $0.4mm$. The distance between the top of the ramp and the collector is $1700mm$. The experiments are performed at the free stream velocity of $U_0 = 30m/s$. The Reynolds number based on the ramp height is $100,000$.

The measurements of the surface fluctuating pressure are obtained with off-set microphones. The inner diameter of the pressure tabs is $0.9mm$ and the bandwidth is $50Hz - 5kHz$. The transfer function of the measurement system is determined with a B&K UA 0922 coupler. The signal recorder is able to save simultaneously 16 pressure probes with an effective sampling frequency of $12.8kHz$ and a cut-off frequency of the anti-aliasing filters set at $6.4kHz$. The Power Spectral

Density (PSD) is estimated with the Welch's method. The time series data is split into segments of 2096 points with a 50% overlap. A Hamming window is used to compute the modified periodogram of each segment. The number of segments is 250. The fluctuating pressure probes (16 probes) used here are on the median axis of the ramp at $x/H = 0{,}2$; 0,3 ; 0,4 ; 0,5 ; 0,6 ; 0,7 ; 0,8 ; 0,9 ; 1,0 ; 1,1 ; 1,2 ; 1,3 ; 1,4 ; 1,6 ; 2,0 ; 4,0.

The velocity measurements are obtained with a two color Laser Doppler Velocimeter. The $476.5nm$ and $496.5nm$ wavelength beams of a argon-ion laser are used to produced the LDV fringe patterns. The estimated size of the measuring volume is less than $0.25mm$ in diameter and $1.3mm$ long in the spanwise direction. The inter-arrival time weighting scheme is used to calculate the mean velocities and Reynolds stresses. $20,000$ velocity samples are recorded at each measurement station and the number of uncorrelated events captured is sufficient to ensure a good statistical convergence.

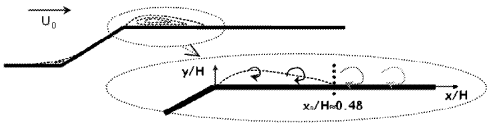

Figure 1: Sketch of the configuration

2 MEAN AND FLUCTUATING VELOCITY FIELDS

In this situation, the ramp is an overwhelming perturbation to the boundary layer. The mean flow speeds up along the ramp. A maximum mean velocity of the order of $U_{max}/U_0 = 1.35$ is measured at $x/H = 0.2$ and $z/H \approx 0.1$. The mean reattachment x_R length is rather small with $x_R/H \approx 0.5$. This value was obtained by detecting the change of sign of the longitudinal mean velocity profile near the wall (at $z/H = 0.01$).

Mean velocity profiles are presented in figure 2a. The acceleration due to the ramp is clearly detected at $x/H = 0.25$ and has nearly disappeared at $x/H = 2.0$. The figure 2b shows that the longitudinal Reynolds stress $\langle u^2 \rangle$ has an important maximum at $x/H = 0.25$; $z/H \approx 0.05$. This normal distance from the wall corresponds to the inflexion point in the mean longitudinal velocity profile at $x/H = 0.25$. Such a high value is both associated with large scale vortices due to the Kelvin Helmoltz instability of the shear layer and to the flapping of the shear layer. We see in figure 2b that this peak decays and diffuses outward as the flow proceeds downstream. There is still a significant outer maximum at $z/H \approx 0.1$ and $x/H = 2.0$ corresponding to four reattachment length. Contrary to the results reported by (Song and al. 2000), $\langle u^2 \rangle$ levels reach a maximum value above the middle of the mean separated region in the present case.

However, we measure a maximum value of $\langle v^2 \rangle$ and $\langle uv \rangle$ at the mean reattachment location $x_R/H \approx 0.5$ (fig. 2c and 2d). Both normal and shear Reynolds stresses then decay rapidly and shift outward for increasing x/H. This behaviour is a common feature in other flows developing subsequent to a reattachment (Alving and Fernholtz 1996; Castro and Epik 1998) and is believed to be associated with the separated shear layer eddies being transported by the mean flow while they dissipate. We will consider the contribution of this out of equilibrium turbulent field on the pressure fluctuations in the rest of the paper.

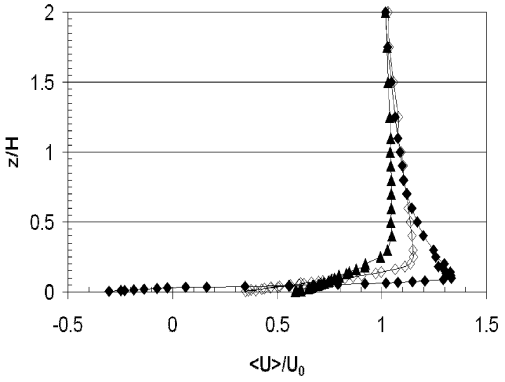

(a) Mean longitudinal velocity $\langle U \rangle$

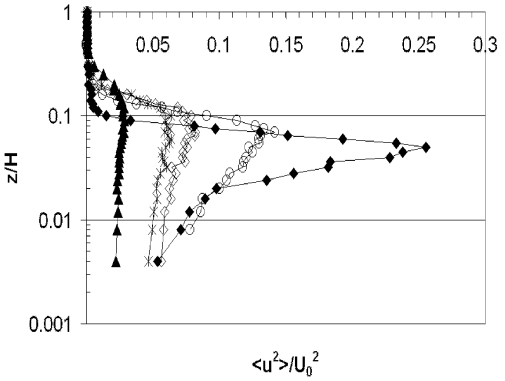

(b) Longitudinal Reynolds stress $\langle u^2 \rangle$

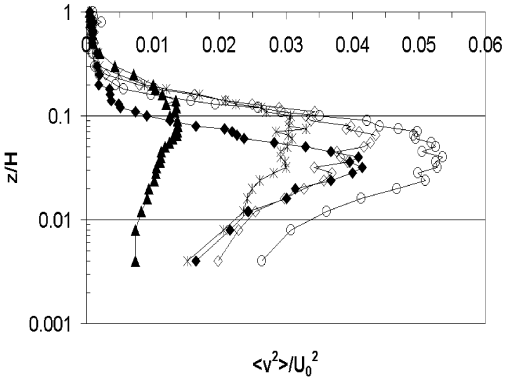

(c) Radial Reynolds stress $\langle v^2 \rangle$

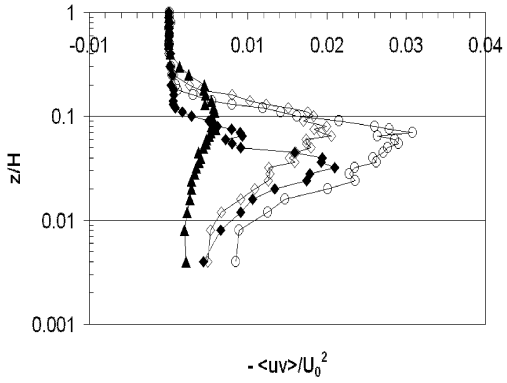

(c) Shear Reynolds stress $\langle uv \rangle$

Figure 2: Mean velocity (a), longitudinal (b), radial (c) and shear (d) Reynolds stresses. ♦, $x/H = 0.25$; ∘, $x/H = 0.50$; ◇, $x/H = 0.80$; ∗, $x/H = 1.00$; ▲, $x/H = 2.00$

3 FLUCTUATING PRESSURE

The figure 3a shows the longitudinal variation of the rms fluctuating pressure coefficient $C_{p'} = \sqrt{\langle p^2 \rangle}/(\rho U_0^2/2)$. The variance of the wall pressure fluctuations is obtained by integrating the wall pressure power spectral density (PSD) from $50Hz$ to $5kHz$. The peak level of $C_{p'}$ is higher than the maximum values measured downstream a fence by (Hudy et al. 2003) or downstream a blunt flat plate by (Cherry et al. 1984). Note that this peak is located upstream the mean reattachment point. The quantity e (right hand side scale) corresponds the cumulated contribution of the sensors to the total variance measured on the sensor array. The separated region clearly dominates.

The PSD of the pressure signal are shown in figure 3b with a semi-log plot. Two maxima are detected at $x/H = 0.2$ and 0.3. On the contrary, a single large band contribution at high frequency is detected further downstream. The low frequency maximum at $x/H \leq 0.3$ has a peak at $f \approx 75Hz$. This corresponds to a Strouhal number $St \approx 0.05$; $St = f \cdot x_R/U_{max}$ is based here on the mean reattachment length and on the maximum mean velocity bounding the separated region. This low frequency wall pressure signature is typically associated with the flapping of the separated shear layer. The high frequency band peaks at $f \approx 1500Hz$ ($St \approx 0.9$). This peak is associated with the shedding of large scale vortical structures from the separated region. The maximum shifts toward lower frequencies when moving downstream. This shift is believed to be due to the decrease of the external mean velocity. The convective characteristics of the surface pressure signal were explored by computing the cross-spectrum for all pressure tabs relative to pressure tab $x/H \leq 0.3$ (peak of $C_{p'}$). The results are not shown here for brevity. The trace of the vortex shedding is clear on a plot of the coherence function in the frequency band . At a given location, the phase angle data plotted as a function of the frequency reveal a linear increase of the phase angle θ with the frequency. A mean convective velocity can be calculated with $U_c = 2\pi \cdot \Delta x \cdot (d\theta/df)^{-1}$. An approximately constant value $U_c \approx 29m/s = 0.72U_{max}$ is obtained for $x/H \leq 1.0$. This is an evidence of a convective motion in the downstream direction associated with vortex shedding.

Our goal is now to decompose the downstream pressure signal so as to extract the contribution of the decaying shear layer structures.

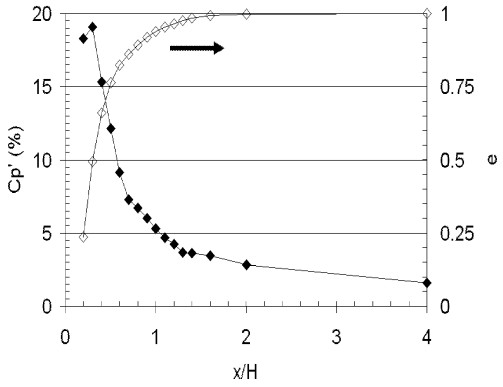

(a) $C_{p'}$

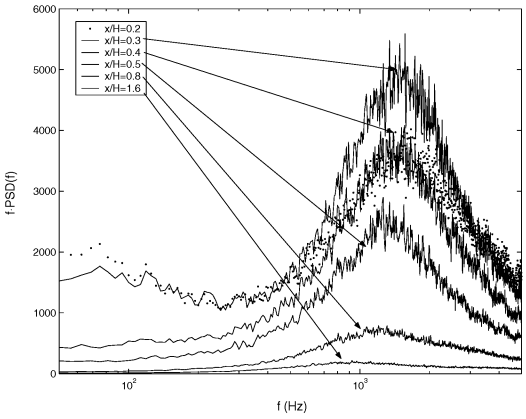

(b) PSD

Figure 3: a, longitudinal variation of the rms fluctuating pressure coefficient $C_{p'}$; b, PSD of the fluctuating pressure

4 POD AND EXTENDED POD ANALYSIS

The proper orthogonal decomposition (POD) was proposed by (Lumley 1967) as an unbiased way for extracting structures in a turbulent flow. In the case considered here, the time direction is homogeneous for the pressure signals. The solution is thus obtained by solving a 1D eigen-value problem for every Fourier mode (Berkooz, Holmes and Lumley 1993; Delville, Cordier and Bonnet 1998). A diagonal decomposition of the cross-spectrum is obtained together with an optimal decomposition of the variance of the fluctuating pressure force integrated over the domain. As the POD is optimal as far as the energy contained in the successive modes is concerned, the analysis has to be performed in energy containing regions, namely under the recirculation bubble for the pres-

sure signal in the present case. The POD problem was solved here by using 5 pressure sensors located from $x/H = 0.2$ to $x/H = 0.6$ (included). This will be called the "POD region" in the following. The figure 3a shows that this region carries more than 82% of the sum of $\langle p^2 \rangle$ over all sensors. From five sensors, we obtain five modes $\hat{\phi}^{(n)}(x_i, f)$ and five real and positive eigenvalues $\lambda^{(n)}(f)$; i=1,..5 is the location of the pressure tabs ; n=1,$\cdots$5 is the rank of the POD mode chosen as $\lambda^{(n)}(f) > \lambda^{(n+1)}(f)$. $\hat{\phi}^{(n)}(x_i, f)$ are the eigenfunctions of the cross-correlation tensor $\Pi(x_i, x_l, f)$ with the main properties :

(i) Orthonormality :

$$(\hat{\phi}^{(n)}, \hat{\phi}^{(p)}) = \sum_{i=1}^{5} \hat{\phi}^{(n)}(x_i, f)\hat{\phi}^{(p)*}(x_i, f) = \delta_{np} \quad (1)$$

(ii) Diagonal representation :

$$\Pi(x_i, x_l, f) = \sum_{n=1}^{5} \lambda^{(n)}(f)\hat{\phi}^{(n)}(x_i, f)\hat{\phi}^{(n)*}(x_l, f) \quad (2)$$

(iii) Optimal decomposition :

$$\sum_{i=1}^{5} \langle p^2 \rangle = \sum_{n=1}^{5} \int \lambda^{(n)}(f) df \quad (3)$$

Each realisation of the random pressure spectrum $\hat{p}_k(x_i, f)$ can be projected onto the POD basis with :

$$\hat{p}_k(x_i, f) = \sum_{n=1}^{5} a_k^{(n)}(f)\hat{\phi}^{(n)}(x_i, f) \quad (4)$$

$$with\ a_k^{(n)}(f) = \left(\hat{p}_k, \hat{\phi}^{(n)}\right) \quad (5)$$

The random coefficients $a_k^{(n)}(f)$ n=1,$\cdots$5 are uncorrelated with $\left\langle a_k^{(n)}(f) a_k^{(p)}(f) \right\rangle = \delta_{np}$, $\langle\ \rangle$ is the ensemble average.

Let's consider now a pressure sensor located downstream the "POD region", at a location x_j (Borée 2003) has shown that each realisation (say n°k) $\hat{p}_k(x_j, f)$ of the pressure spectrum at x_j can be exactly decomposed into two parts $\hat{p}_{Ck}(x_j, f)$ and $\hat{p}_{Dk}(x_j, f)$ respectively correlated and uncorrelated to the pressure signal in the "POD region". It comes simply :

$$\hat{p}_k(x_j, f) = \hat{p}_{Ck}(x_j, f) + \hat{p}_{Dk}(x_j, f) \quad (6)$$

$$\hat{p}_{Ck}(x_j, f) = \sum_{n=1}^{5} a_k^{(n)}(f)\hat{\Psi}^{(n)}(x_j, f) \quad (7)$$

$\hat{\Psi}^{(n)}(x_j, f)$ is the deterministic extended mode and :

$$\hat{\Psi}^{(n)}(x_j, f) = \left\langle \hat{p}_k(x_j, f) \cdot a_k^{(n)*}(f) \right\rangle / \lambda^{(n)}(f) \quad (8)$$

Note that $\hat{\Psi}^{(n)}(x_j, f)$ coincides with the POD mode $\hat{\phi}^{(n)}(x_j, f)$ if x_j belongs to the POD region.
The demonstration not recalled here is natural and uses the fact that the random coefficients $a_k^{(n)}(f)$ are uncorrelated. Moreover, we obtain a mode to mode decomposition of $\hat{p}_{Ck}(x_j, f)$ and an interesting decomposition of $\Pi(x_i, x_j, f) = \sum_{n=1}^{5} \lambda^{(n)}(f)\hat{\phi}^{(n)}(x_i, f)\hat{\Psi}^{(n)*}(x_j, f)$ for x_i belonging to the POD region.

The evolution of the five POD λ-spectrum is shown in figure 4. The first mode carries 71% of the total energy integrated over the frequency domain. Both flapping and vortex shedding mechanisms contribute to this first mode in a frequency domain dominated by $x/H = 0.2$ and $x/H = 0.3$ sensors. The mode 2 contributes to 15% of the total energy, mainly in the frequency band associated with the vortex shedding. A mode by mode decomposition of the coherence confirms that modes 1 and 2 are associated with large scale events while higher order modes 3, 4 and 5 correspond to smaller scale events not resolved by our coarse spatial discretisation.

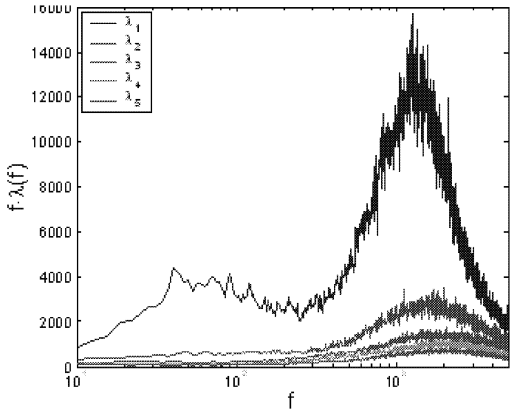

Figure 4: Evolution of the five POD λ-spectrum

We now examine the results of an EPOD decomposition at downstream locations. The power density spectra of respectively $\hat{p}(x_i, f)$, $\hat{p}_C(x_i, f)$ and $\hat{p}_D(x_i, f)$ at $x/H = 0.7$, 0.8 and 1.0 are shown in figure 5. The high frequency region is dominated by the uncorrelated part. On the contrary, the correlated part always display a peak in the frequency domain associated with vortex shedding. Moreover, as this correlated part is the only contributor to the cross-spectrum between the POD region and these locations, a study of the phase angle evidence the convective nature of the pressure signal in the shedding frequency band as discussed in part 3.

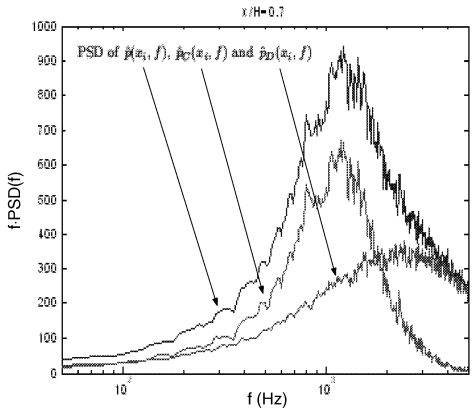

(a) At $x/H = 0.7$

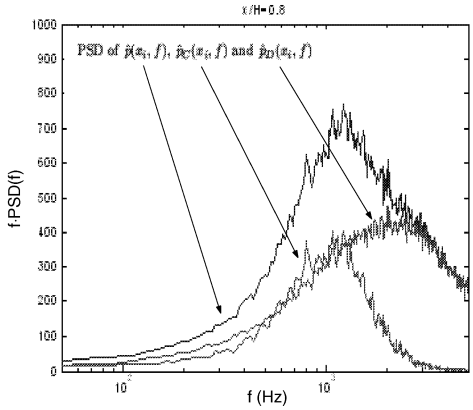

(b) At $x/H = 0.8$

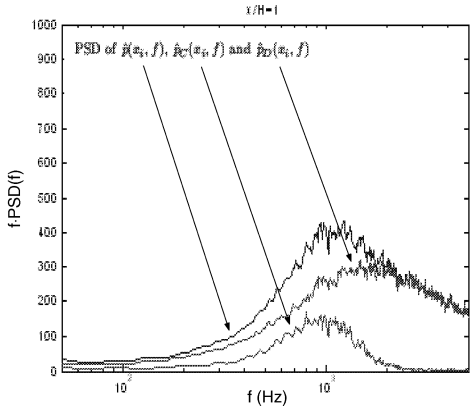

(c) At $x/H = 1.0$

Figure 5: Power density spectra of respectively $\hat{p}(x_i, f)$, $\hat{p}_C(x_i, f)$ and $\hat{p}_D(x_i, f)$ at $x/H = 0.7$, 0.8 and 1.0

In the POD region, the main contribution to the fluctuating pressure signal is believed to be associated with the large scale shear layer vortices (valleys) and by inrush of external fluid moving toward the wall (peaks) as described by (Kiya and Sasaki 1985). The rate at which their contribution to the pressure signal decays when moving downstream should therefore be associated with the rate at which these structures dissipate once embedded in the outer region of the recovering boundary layer (Castro and Epik 1998). In a first approximation, focussing on the hydrodynamic (as opposed to acoustic) contribution of the turbulent field on the wall pressure signal, it seems natural to search for a scaling of the decay of the quantity $w_c(x/H) = \left[\left\langle p_C^2 \right\rangle (x/H)/\rho^2\right]^{1/4}$, ρ is the air density. $w_c(x/H)$ is a decaying velocity scale associated with the decaying correlated pressure field. We defined $w_{c0} = w_c(x/H = 0.5)$ and the ratio $w_{c0}/w_c(x/H) = \left[\left\langle p_C^2 \right\rangle (x/H = 0.5)/\left\langle p_C^2 \right\rangle (x/H)\right]^{1/4}$ is drawn in figure 6. $x/H = 0.5$ was selected as a reference position because it is the end of the mean separated region. In the POD region, $\left\langle p_C^2 \right\rangle$ is by definition equal to $\left\langle p^2 \right\rangle$. Further downstream, for $x/H > 0.6$, $\left\langle p_C^2 \right\rangle$ becomes much smaller than $\left\langle p^2 \right\rangle$ as evidenced in the figure 6. It is interesting to note that $w_{c0}/w_c(x/H)$ has a linear evolution from the end of the mean separated region up to three time the mean reattachment length at $x/H = 1.5$. The slope of the straight line obtained by a linear regression is $s = 2.32$. A simple physical model for $k_c = 3/2(w_c)^2$ can be built by assuming that, downstream the mean separated region, the shear layer vortical structures, of size $l \approx 0.1H$ (see fig. 2) dissipate while being advected at the mean velocity $U_c \approx 29m/s = 0.72U_{max}$ determined previously. One gets :

$$U_c \frac{dk_c}{dx} = -\frac{k_c^{3/2}}{l} \tag{9}$$

$$(9) \;\Rightarrow\; \frac{w_{c0}}{w_c}(x/H) = 1 + \alpha \frac{H\sqrt{k_{c0}}}{l \cdot U_c}\left(\frac{x - x_0}{H}\right) \tag{10}$$

α is a constant which should be of order one. k_{c0} is estimated at $x/H = 0.5$ by $k_{c0} = k_{max} \approx \left(\left\langle u^2 \right\rangle + 2\left\langle v^2 \right\rangle\right)/2$ with $\left\langle u^2 \right\rangle/(U_0)^2 = 0.13$ and $\left\langle v^2 \right\rangle/(U_0)^2 = 0.05$ (see fig. 2b and 2c).

If we identify the slope s in fig. 6 and the analytical result, one gets $s = \alpha\frac{H\sqrt{k_{c0}}}{l \cdot U_c}$ for $\alpha = 0.7$. Owing to the approximation involved in this simple physical model, we believe that this result shows that the correlated part of the pressure signal is indeed the trace of the decaying remnants of the large scale shear layer vortices. Being able to extract such contribution from the complex pressure trace in the recovering boundary layer may be important for further application of this technique.

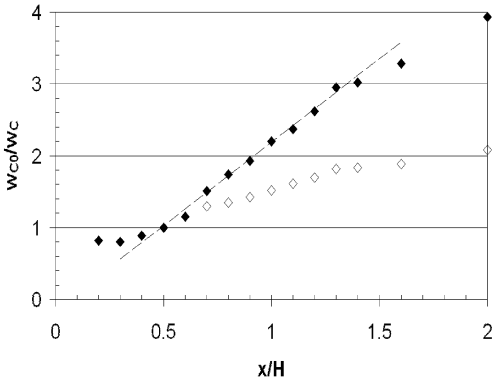

Figure 6: Evolution of
♦, $w_{c0}/w_c(x/H) = \left[\left\langle p_C^2 \right\rangle (x/H = 0.5)/\left\langle p_C^2 \right\rangle (x/H)\right]^{1/4}$
⋄, $\left[\left\langle p^2 \right\rangle (x/H = 0.5)/\left\langle p^2 \right\rangle (x/H)\right]^{1/4}$

5 CONCLUSION

Wall pressure array measurements and single point measurements of the velocity using two components LDV obtained on a 30° forward facing ramp were discussed in this paper. Mean and fluctuating velocity and pressure signals were first analysed both in the separated region and in the recovering boundary layer flow. The signature of the large scale separated shear layer eddies is clear and in aggreement with classical references concerning other flows developing subsequent to a reattachment. An analysis of the phase angle of the cross spectrum provides an evidence of the convective motion in the downstream region associated with vortex shedding. Note that a signature of flapping is detected immediately downstream separation.

POD technique is a natural tool to analyse the multipoint pressure measurements. The variance of the fluctuating pressure is however very non homogeneous: high in the separated region and low in the recovering boundary layer. The "POD region" is therefore restricted to the mean separated region where the pressure trace is dominated by the signature of large vortical structures. Extended POD is then used to educe the length and time scale contribution of these decaying structures on the pressure trace downstream of separation. We prove that the correlated pressure signal downstream mean separation length carries the properties of distorded mixing layer eddies being advected and dissipating in the outer boundary layer flow. A physical model is proposed accordingly. It validates these statements and establishes a clear statistical link between pressure and velocity data acquired independently. Being able to extract such contribution from the complex pressure trace in the recovering boundary layer may be important for further application of this technique in the aero-acoustic or fluid/structure interaction domains.

ACKNOWLEDGEMENTS

The set-up used here was built in the context of a National Research group *"Recherche en Aérodynamique et Aéroacoustique pour les véhicules terrestres"* supported by Renault SA and PSA Peugeot-Citroen.

We thank Professor J.-C. Valière for fuitfull discussions. The technical support of P. Braud and L. Phillipon is greatly acknowledged. We thank the staff of the LEA mechanical workshop.

REFERENCES

Alving, A. E. and Fernholtz, H. H. (1996). Turbulence measurements around a mild separation bubble and downstream of reattachment. J. Fluid Mech. 322: 297-328.

Berkooz, G., Holmes, P. and Lumley, J. L. (1993). The proper orthogonal decomposition in the analysis of turbulent flows. Ann. Rev. Fluid Mech. 25: 539-575.

Borée, J. (2003). Extended proper orthogonal decomposition: a tool to analyse correlated events in turbulent flows. Exp. in Fluids 35: 188-192.

Castro, I. P. and Epik, E. (1998). Boundary layer development after a separated region. J. Fluid Mech. 374: 91-116.

Cherry, N. J., Hillier, R. and Latour, M. (1984). Unsteady measurements in a separated and reattaching flow. J. Fluid Mech. 144: 13-46.

Delville, J., Cordier, L. and Bonnet, J. P. (1998). Large scale structure identification and control, Flow Control - Fundamental and Practices eds. M. Gad-el-Hak, A. Pollard, J.P. Bonnet, Springer.

Eaton, J. K. and Johnston, J. P. (1981). A review of research on subsonic turbulent flow reattachement. AIAA Journal 19: 1093-1100.

Hudy, L. M., Naguib, A. N. and Humphreys, W. M. (2003). Wall-pressure-array measurements beneath a separating/reattaching flow region. Phys. of Fluids 15-3: 706-717.

Kiya, M. and Sasaki, K. (1983). Structure of a turbulent separation bubble. J. Fluid Mech. 137: 83-113.

Kiya, M. and Sasaki, K. (1985). Structure of large scale vortices and unsteady reverse flow in the reattaching zone of a turbulent separation bubble. J. Fluid Mech. 154: 463-491.

Lee, I. and Sung, H. J. (2002). Multiple-arrayed pressure measurement for investigation of the unsteady flow structure of a reattaching shear layer. J. Fluid Mech. 463: 377-402.

Lumley, J. L. (1967). The structure of inhomogeneous turbulence. Atmospheric turbulence and radio wave propagation.

Song, S., DeGraff, D. B. and Eaton, J. K. (2000). Experimental study of a separating, reattaching, and redeveloping flow over a smoothly contoured ramp. Int. Jour. of Heat and Fluid flow 21: 512-519.